Science Advances
AAAS

Supplementary Materials for

Antagonistic effect of cyclin-dependent kinases and a calcium-dependent phosphatase on polyglutamine-expanded androgen receptor toxic gain of function

Diana Piol *et al.*

Corresponding author: Maria Pennuto, maria.pennuto@unipd.it, pennutom@gmail.com;
Laura Tosatto, laura.tstt@gmail.com

Sci. Adv. **9**, eade1694 (2023)
DOI: 10.1126/sciadv.ade1694

The PDF file includes:

Other Supplementary Material for this manuscript includes the following:

Tables S1 to S3

Supplementary Table S1. PolyQ expansion does not modify phosphorylation sites on androgen receptor. A) Mass spectrometry analysis of androgen receptor 24Q and 65Q, reporting sequence coverage, the peptide list of corresponding to androgen receptor fragments and the areas of peaks related to the main phosphorylation sites. B) List of tryptic peptides of AR24Q identified by mass spectrometry. C) List of tryptic peptides of AR65Q identified by mass spectrometry.

Supplementary Table S2. Selective kinase inhibitors are able to modulate AR65Q biology. Kinase inhibitors chemical information and statistics on data reported in Figure 3A and 3B.

S**upplementary Table S3. Selective phosphatase inhibitors are able to modulate AR65Q biology.** Phosphatase inhibitors chemical information and statistics on data reported in Figure 4A.

Figs. S1 to S8

Fig. S1. Sequence alignment of AR from species of the kingdom Animalia.

Fig. S2. Loss of either S83 or S651 phosphorylation does not affect phosphorylation at the other major phosphosites.

Fig. S3. High-throughput screen of kinase inhibitors.

Fig. S4. High-throughput screening of kinase inhibitors.

Fig. S5. Kinase drug inhibitors identify cellular pathways as modifiers of polyQ-expanded AR nuclear accumulation.

Fig. S6. High-throughput screening of phosphatase inhibitors.

Fig. S7. CDC25 and CDK2 inhibition is protective in cells expressing polyQ-expanded AR.

Fig. S8. CDK2 ablation reduces polyQ-expanded AR accumulation in the spinal cord but not skeletal muscle of SBMA mice.

Fig. S1.

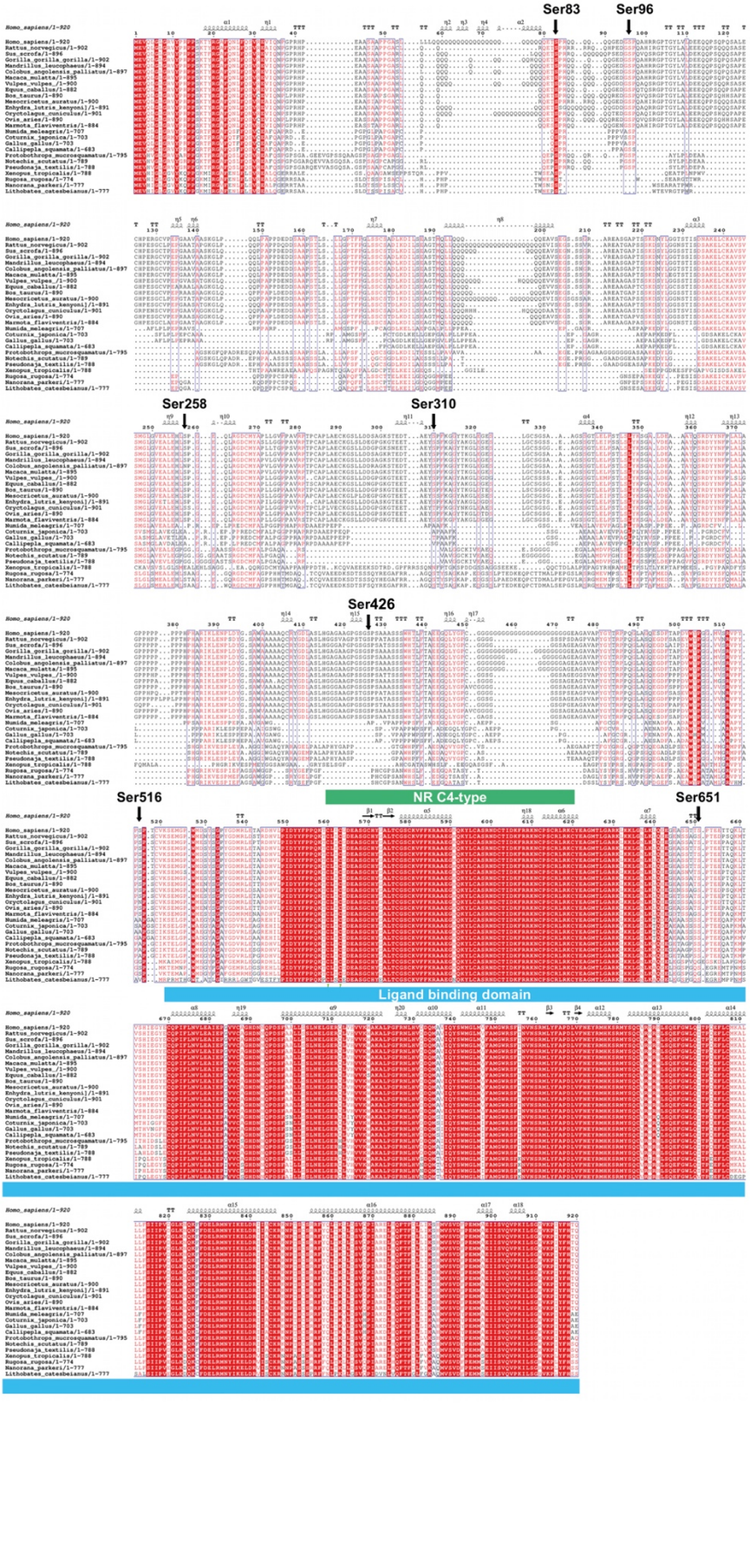
Ser83
Ser96
Ser258
Ser310
Ser426
Ser516
NR C4-type
Ser651
Ligand binding domain

Fig. S1. Sequence alignment of AR from species of the kingdom Animalia. Conserved amino acids are highlighted in red. NR-C4 type zinc finger is indicated in green. SP sites are marked along the sequence with black arrows.

Fig. S2

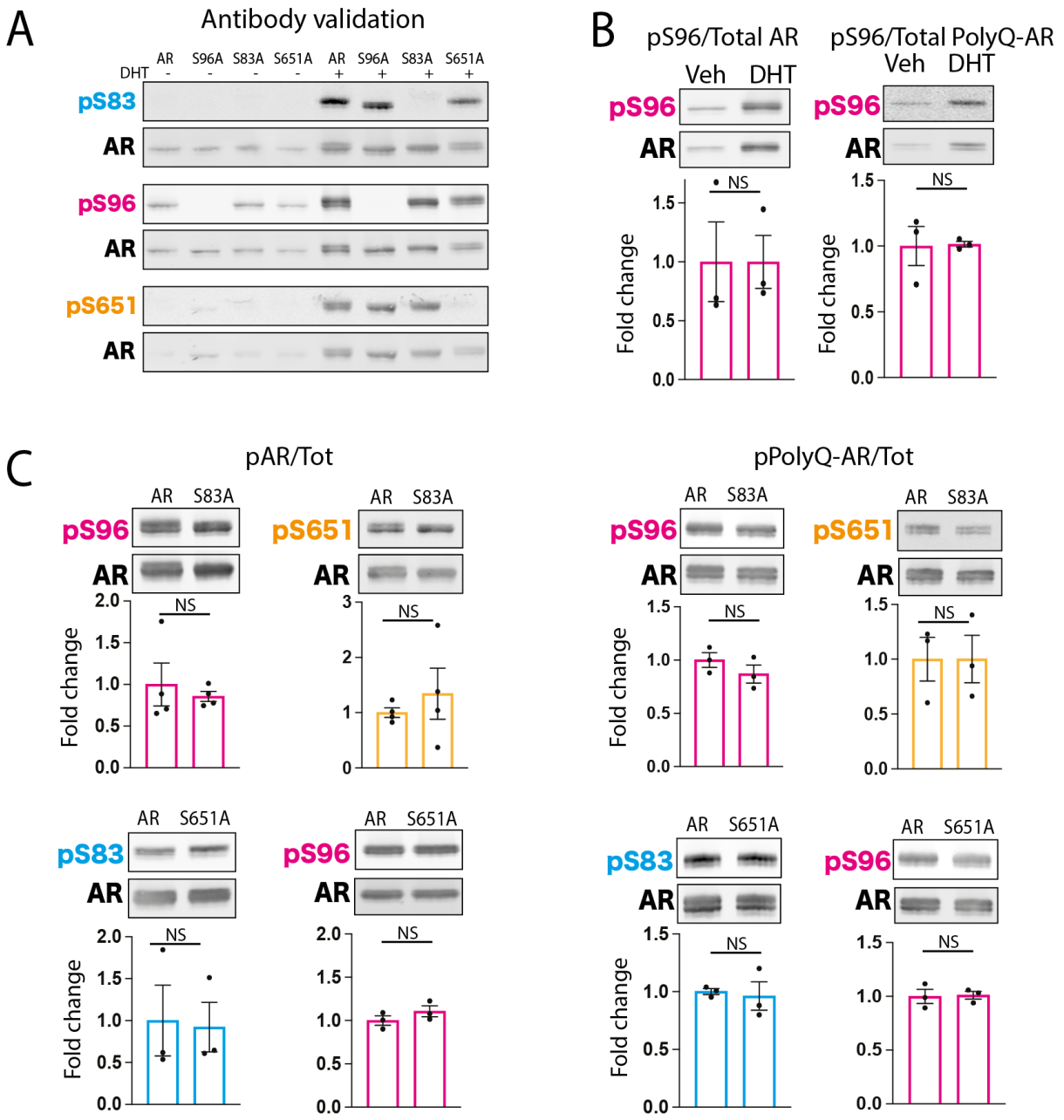

Fig. S2. Loss of either S83 or S651 phosphorylation does not affect phosphorylation at the other major phosphosites.

A) Western blot analysis of AR12Q phosphorylation at S83, S96, and S651 in HEK293T cells expressing the phosphomutants S96A, S83A, and S651A for phosphosite specific antibody validation. Cells were treated with and without DHT (10 nM, 24 h). AR phosphorylation at specific sites was analyzed with phospho-specific antibodies recognizing the indicated serine residue when phosphorylated. Antibody specificity was based on recognition of the phospho-defective alanine mutant. Total AR was detected with a specific antibody recognizing the protein independently of phosphorylation.

B) Western blot analysis of the phosphorylation status of nonexpanded AR (AR12Q) and polyQ-expanded AR (AR55Q) in HEK293T cells treated with vehicle (Veh) and DHT (10 nM, 24 h) (n = 3 biological replicates).
C) Western blot analysis of the phosphorylation status of nonexpanded AR (AR12Q) and polyQ-expanded AR (AR55Q) phospho-defective variants in HEK293T cells treated with DHT (10 nM, 24 h) (n = 3-4 biological replicates).

Phosphorylated AR was detected using phospho-specific antibodies and total AR was detected with a specific antibody. Graphs show mean ± SEM, two-tailed Student t-test. NS, nonsignificant

Fig. S3

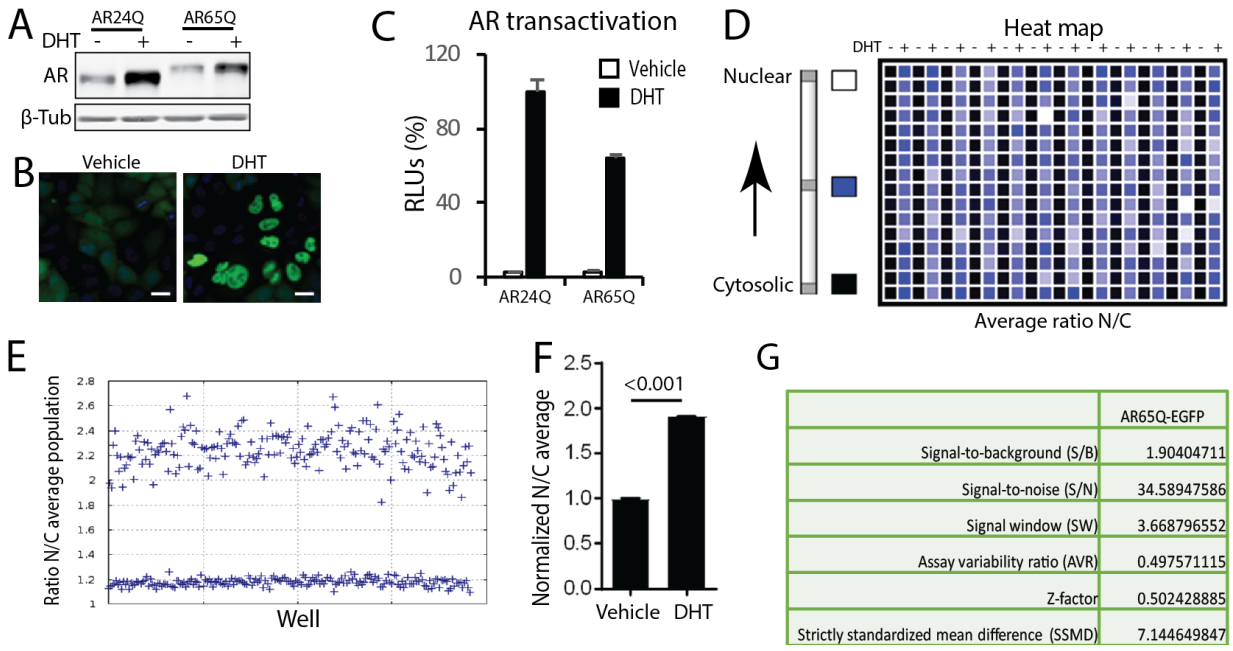

	AR65Q-EGFP
Signal-to-background (S/B)	1.90404711
Signal-to-noise (S/N)	34.58947586
Signal window (SW)	3.668796552
Assay variability ratio (AVR)	0.497571115
Z-factor	0.502428885
Strictly standardized mean difference (SSMD)	7.144649847

Fig. S3. High-throughput screen of kinase inhibitors.

A) Western blot analysis of HeLa cells stably expressing AR24Q-EGFP and AR65Q-EGFP, treated with or without DHT (10 nM, 24 h). Image is representative of at least n = 3 biological replicates. AR was detected with a specific antibody and beta-Tubulin (β-tub) was used as loading control.

B) Representative fluorescence images of AR65Q-EGFP (green) stably expressed in the HeLa cells treated with and without DHT (10 nM, 4 h) (n = 3 biological replicates). Scale bar, 25 μm.

C) Transcriptional assay performed in HeLa cells stably expressing AR24Q-EGFP and AR65Q-EGFP treated with and without DHT (10 nM, 24 h) (n = 3 biological replicates). RLUs: relative luminescence units.

D) Preliminary high-throughput screening. HeLa cells expressing AR65Q-EGFP were treated with and without DHT (10 nM, 4 h). The color-coded indication of more cytosolic (black), more nuclear (white) or equal (blue) localization is represented for every well in 384-well plate format. Odd columns were treated with vehicle, even columns with DHT.

E) Nuclear versus cytosolic EGFP intensity ratio (N/C) of the average population of single wells.

F) Normalized quantification of N/C polyQ-expanded AR subpopulation in the preliminary high-throughput screen (n = 192 wells/each condition).

G) Quality and robustness parameters of the high-throughput preliminary screen of kinase and phosphatase inhibitors.

Graphs show mean ± SEM, two-tailed Student t-test.

Fig. S4

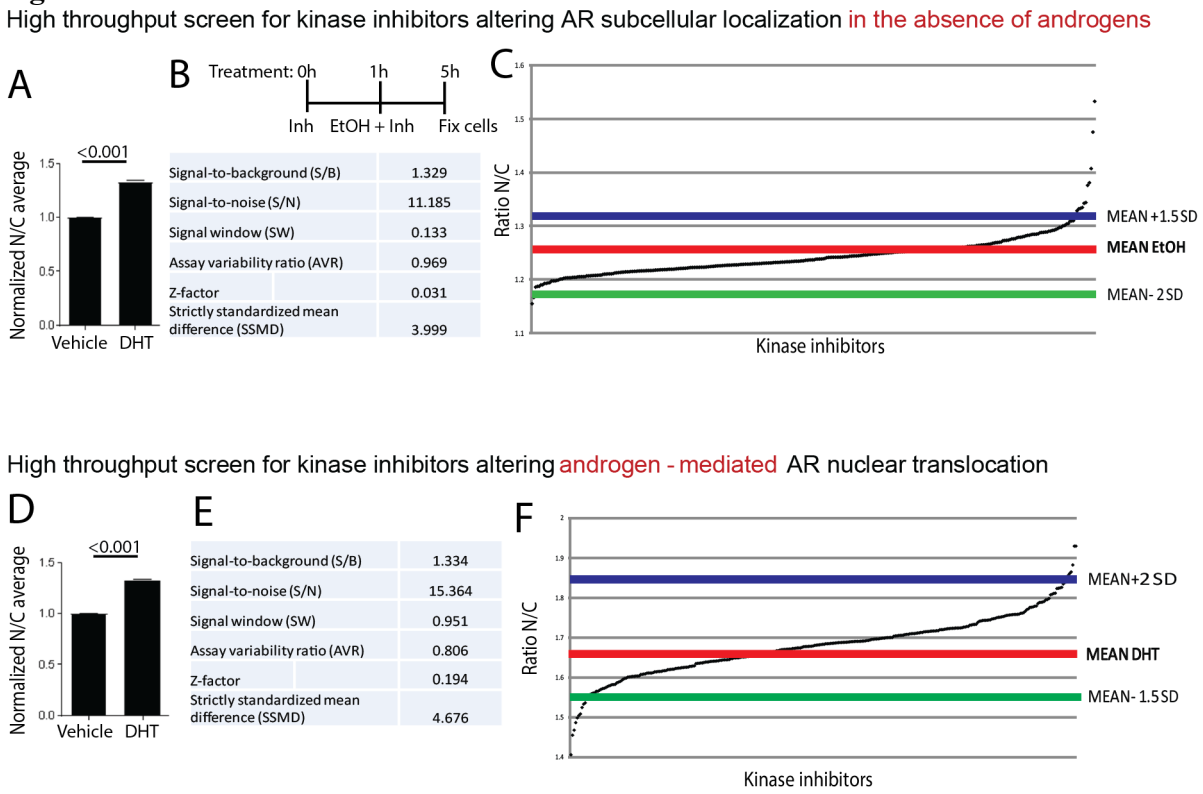

Fig. S4. High-throughput screening of kinase inhibitors.

A) Normalized quantification of N/C ratio of AR65Q-EGFP cell subpopulation in high-throughput screening with kinase inhibitors performed in cells treated with vehicle (EtOH, n = 96) and the indicated inhibitors (n = 3).

B) Experimental workflow showing treatment of HeLa cells with kinase inhibitors (Inh, 10 µM, 5 h). One hour after adding inhibitors, EtOH was added. The table below reports the quality and robustness parameters of the high-throughput screen of kinase inhibitors.

C) Graphical representation of the bulk results of the high-throughput screening. The average N/C ratio is plotted for each compound. The red line represents the mean N/C of the EtOH-treated samples, used as control. The blue line represents 1.5-fold the standard deviation (SD) of the mean N/C of the EtOH-treated cells, and green line 2-fold the SD.

D) Normalized quantification of N/C ratio of AR65Q-EGFP^{+} cell subpopulation in the high-throughput screen with kinase inhibitors performed in cells treated with DHT (n = 96 wells per condition).

E) Experimental workflow involving treatment of HeLa cells with kinase inhibitors (Inh, 10 µM, 5 h) and DHT treatment was as in (B). The table displays the quality and robustness parameters of the high-throughput screening of kinase inhibitors.

F) Graphical representation of bulk results of the high-throughput screening. The average N/C ratio is plotted for each compound. The red line represents the mean N/C of the DHT-treated wells, used as control. The blue line represents 2-fold the SD and the green line 1.5-fold the SD.

Graphs show mean ± SEM, two-tailed Student t-test.

Fig. S5

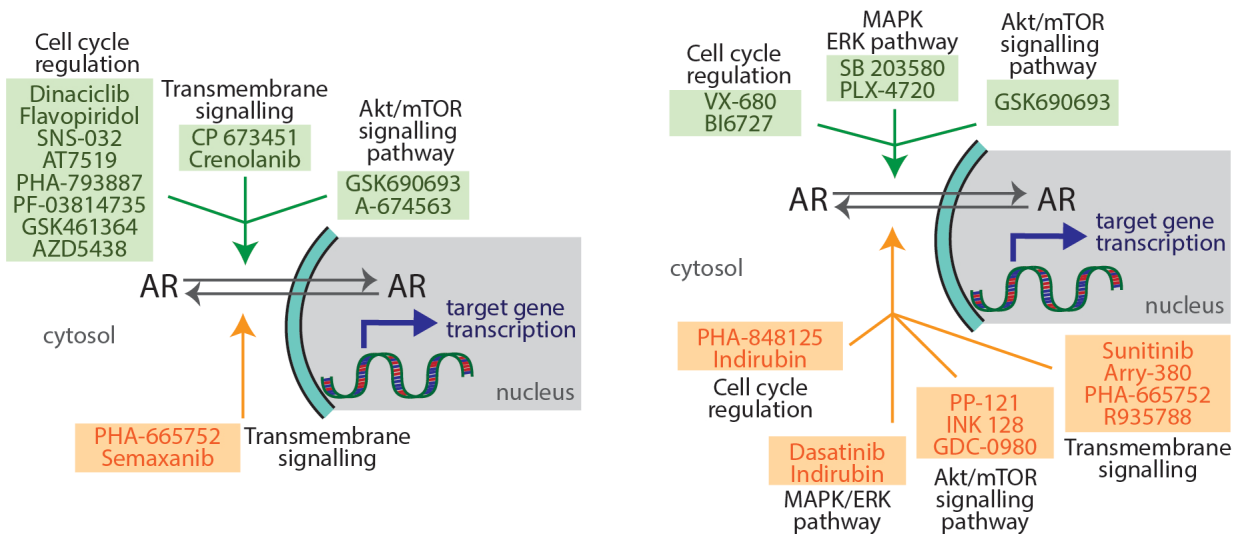

Fig. S5. Kinase drug inhibitors identify cellular pathways as modifiers of polyQ-expanded AR nuclear accumulation.

Compounds increasing nuclear localization in the absence of androgens (left panel) and presence of androgens (right panel) are shown in green, and include molecules targeting cell cycle regulation, mTOR/Akt signaling pathway, transmembrane signaling and MAPK/ERK pathway.

Fig. S6

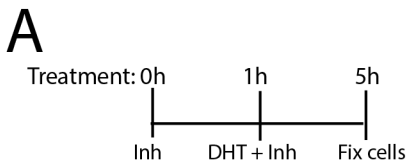

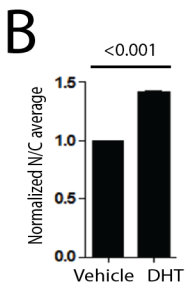

C

Signal-to-background (S/B)	1.418
Signal-to-noise (S/N)	22.979
Signal window (SW)	4.590
Assay variability ratio (AVR)	0.474
Z-factor	0.526
Strictly standardized mean difference (SSMD)	8.160

Fig. S6. High-throughput screening of phosphatase inhibitors.

A) Experimental workflow showing treatment of HeLa cells with phosphatase inhibitors (Inh, 10 μM, 5 h). After 1 h from the addition of the inhibitors, the cells were treated with DHT (10 nM).

B) Normalized quantification of nuclear versus cytosolic (N/C) GFP intensity of AR65Q-EGFP cell subpopulation in the high-throughput preliminary screening of phosphatase inhibitors (n = 12 wells per condition).

C) Quality and robustness parameters of the high-throughput preliminary screen of phosphatase inhibitors.

Graphs show mean ± SEM, two-tailed Student t-test.

Fig. S7

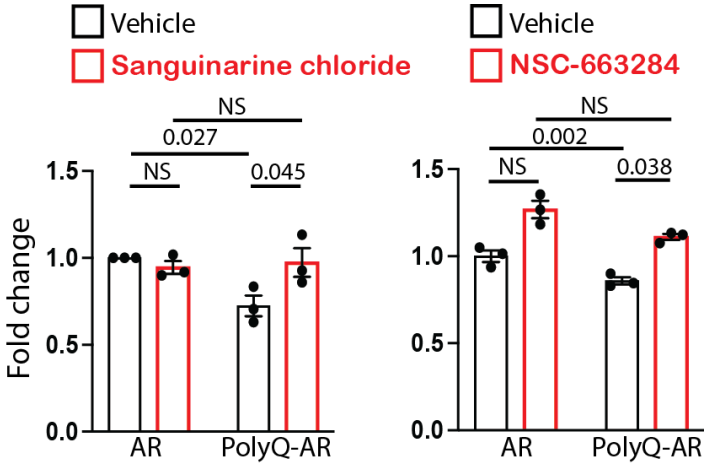

Fig. S7. CDC25 and CDK2 inhibition is protective in cells expressing polyQ-expanded AR. MTT cell viability assays performed in HEK293T cells transfected with vectors expressing AR24Q and AR65Q and treated with DHT (10 μM, 48 h). For the last 18 hours, cells were treated with vehicle or sanguinarine chloride (0.1 μM) and NSC-663284 (1 μM), (n = 3 biological replicates). Graphs show mean ± SEM, two-way ANOVA followed by Tukey's HSD test.

Fig. S8

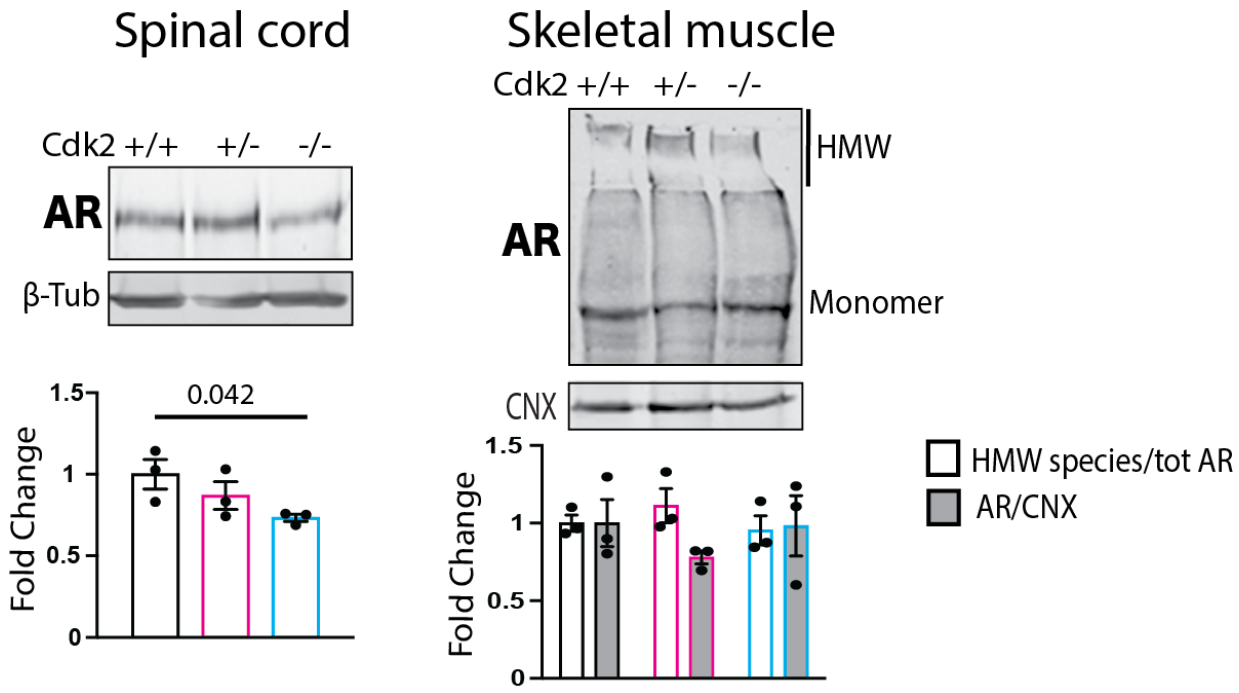

Fig. S8. CDK2 ablation reduces polyQ-expanded AR accumulation in the spinal cord but not skeletal muscle of SBMA mice.

Western blot of AR in the spinal cord and skeletal muscle (quadriceps) of 8-week-old AR100Q/CDK2$^{+/+}$, AR100Q/CDK2$^{+/-}$, AR100Q/CDK2$^{-/-}$ male mice, n = 2-3 mice/genotype. Graphs show mean ± SEM, one-way ANOVA followed by Tukey's HSD test.